Direct-reaction plus statistical-model analysis of the $^{52}Cr(d,2n)^{52}Mn^{g,m}$ reaction

M. G. Mustafa and T. Tamura*
Lawrence Livermore National Laboratory, University of California, Livermore, California 94550

T. Udagawa
Department of Physics, University of Texas, Austin, Texas 78712
(Received 24 November 1986)

Recent experimental cross sections for the reaction $^{52}Cr(d,2n)^{52}Mn^{g,m}$ are in marked disagreement with the standard statistical-model analysis. We have, therefore, analyzed the data with an approach that emphasizes direct-reaction contribution to the cross section. This is done in two steps. In the first step, the compound-nucleus formation cross section is defined such that only the internal part of the target nucleus is allowed to absorb the deuteron, thus leading to the formation of $^{54}Mn^*$. The contribution of the external part is interpreted as going to direct reaction. The calculation of the internal part then proceeds by statistical evaporation of two neutrons to produce ^{52}Mn. In the second step, the dominant part of the direct reaction, i.e., the deuteron breakup, followed by the capture of the proton, is considered. This quantum mechanical, breakup fusion process forms $^{53}Mn^*$, which then evaporates one neutron to produce ^{52}Mn. The sum of the cross sections from these two processes fits the data quite well. The consistency of this twofold treatment is confirmed by our finding that the total reaction cross section for the deuteron is accounted for by summing the above two fusion cross sections with the additional direct-reaction cross sections that do not contribute to the production of ^{52}Mn.

I. INTRODUCTION

Recently excitation functions were measured[1] using foil activation methods for two reactions: $^{52}Cr(p,n)^{52}Mn^{g,m}$ and $^{52}Cr(d,2n)^{52}Mn^{g,m}$. These data were then analyzed by the statistical model (SM) approach.[1] It was found that the model fits the (p,n) data very nicely, but not the (d,2n) data. The purpose of this paper is to explain the discrepancy in the (d,2n) data.

The experiment measured $\sigma(g)$ and $\sigma(m)$, which are, respectively, the cross sections for forming the ground 6^+ and the isomeric 2^+ (378 keV) states in ^{52}Mn. We shall call $\sigma=\sigma(g)+\sigma(m)$ the combined ^{52}Mn-formation cross section and call $R=\sigma(m)/\sigma(g)$ the isomer ratio. As shown in Ref. 1, the trouble with the standard statistical model (SSM) with two particle—one hole as the initial exciton configuration in the preequilibrium model is that the theoretical (d,2n) cross section, σ_{theor}, exceeds the experimental cross section, σ_{expt} by 30—50%. The agreement is better with the choice of 2p-0h initial exciton configuration, but becomes worse with 3p-1h configuration. Also, for the deuteron energy $E_d \gtrsim 10$ MeV, the value of the isomer ratio is found experimentally to be roughly unity, while for theory R is less than 0.5 and is insensitive to the choice of the initial exciton configuration. We want to remove these two difficulties. (For additional discussion on SSM, see Sec. III A.)

As is well known, the SM method first calculates σ_I, the cross section with which a compound nucleus with spin I is formed. It then calculates the ensuing decay process. In the SSM method, one uses as σ_I the spin I part of the total reaction cross section, σ_R, which is obtained from the optical model, $\sigma_R=\sum_I \sigma_I$. The successful (p,n) analysis made in Ref. 1 shows that this SSM approach is quite acceptable when the projectile is a proton. When the projectile is a deuteron, however, the situation is different.

The fact that σ_{theor} exceeds σ_{expt} for (d,2n) suggests that the value for σ_I used in the SSM is too large (at least for a range of I), but acutally we should not be surprised at this fact. Note that the total reaction cross section σ_R contains two parts. The first, σ_R^F, is associated with fusion of the projectile with the target (i.e., σ_R^F is the formation cross section of the compound nucleus) and the second, σ_R^{DR}, is responsible for direct reactions. Since the deuteron is easily broken up, σ_R^{DR} is expected to be rather large in deuteron-induced reactions. Thus, σ_R^F is expected to be significantly smaller than the total reaction cross section σ_R.

If the spin I part of σ_R^F is now used as σ_I in the SM calculation for the (d,2n) reaction, σ_{theor} will be reduced and the first of the difficulties encountered in Ref. 1 will be overcome. In Sec. II A, we present a very simple method of achieving such a reduction. This method, which we call the direct-reaction approach to fusion (DRAF), was used very successfully in fitting the cross sections for fusion between two heavy ions, both below and above the Coulomb barrier.[2]

The DRAF method is, however, phenomenological. In particular, it does not calculate the cross section for the breakup, but only considers its possible onset conceptually. Explicit calculations of the breakup cross section, and calculations of the breakup fusion cross section, are reserved for Sec. II B.

When one speaks of the breakup of the deuteron, one

normally has in mind the process during which both the proton and the neutron fly apart. In the simplest case of this process, which we call elastic breakup (EB), the target stays in its ground state. The EB cross section should be an important component of $\sigma_R^{\rm DR}$.

A straightforward calculation of the EB cross section is normally performed when one wants to fit data for which protons and neutrons are measured in coincidence. On many occasions, however, the experiment measures only the neutrons or protons separately, i.e., it measures only the singles cross sections. Let us, for the sake of definiteness, consider the neutron- (n) singles cross section. This is obtained by integrating the above EB cross section over all of the proton degrees of freedom. It is now well known,[3–7] however, that this n-singles contribution is rather small, and that a major contribution to the n-singles cross section comes from a process called breakup fusion (BF).[4–7] Here the EB process is followed by the absorption of the proton by the target.

In Sec. II B we explain the calculation of the BF as well as the EB cross sections in some detail. The reason for doing this is not simply that the BF process makes a large contribution to the n-singles cross section. It is because the BF process followed by evaporation (which we call the BFE process) contributes importantly to the (d,2n) cross section.

In Sec. II C, we explain how the SM calculations follow from the results of Secs. II A and II B.

Numerical results are presented in Sec. III. Section III A discusses the basics of the statistical model calculation, and this discussion is followed in Sec. III B by calculations using the DRAF method. The BF calculation is made in Sec. III C, and consistency arguments are given in Sec. III D to justify the use of the DRAF method. Our overall work in SSM, DRAF, and BFE is summarized in Sec. IV.

II. THEORETICAL FORMALISM

A. Direct-Reaction approach to fusion (DRAF) method

As shown in Ref. 2, the total reaction cross section σ_R for an incident deuteron can be written as

$$\sigma_R=(2\pi/\hbar v_{\rm d})(\langle\chi_{\rm d}^{(+)}\,|\,W_{\rm d}\,|\,\chi_{\rm d}^{(+)}\rangle/\pi)\ , \tag{1}$$

where $v_{\rm d}$ is the deuteron velocity, $\chi_{\rm d}^{(+)}$ is the deuteron distorted wave, and $W_{\rm d}$ is the negative of the imaginary part of the deuteron optical potential.

The distorted wave $\chi_{\rm d}^{(+)}$ can be expanded into partial waves as

$$\chi_{\rm d}^{(+)}=(1/k_{\rm d}r)\sum_{l=0}^{\infty} i^l(2l+1)\chi_l(r)P_l(\theta)\ , \tag{2}$$

where $k_{\rm d}$ is the wave number. The function $P_l(\theta)$ is the Legendre polynomial. By using Eq. (2), expression (1) can be rewritten as

$$\sigma_R^{\rm OM}=(\pi/k_{\rm d}^2)\sum_{l=0}^{\infty}(2l+1)T_l^{\rm OM}\ , \tag{3}$$

with the transmission coefficient $T_l^{\rm OM}$ given by

$$T_l^{\rm OM}=(8/\hbar v_{\rm d})\int_0^{\infty}|\chi_l(r)|^2 W_{\rm d}(r)dr\ . \tag{4}$$

Note that we have attached superscript OM to $\sigma_R^{\rm OM}$ and $T_l^{\rm OM}$ to emphasize their optical-model (OM) origin.

Equations (2)–(4) were obtained by assuming that the deuteron has no spin, a simplification that is well justified for the purpose of this paper. (Contributions from different $\mathbf{j}=\mathbf{l}+\mathbf{s}$ with a given l will average out.) Since the target ^{52}Cr is in a 0^+ state, the spin I of the compound nucleus ^{54}Mn* is the same as the orbital angular momentum l of the partial wave that is responsible for forming the compound nucleus. Thus, the partial cross section for creating this compound state is written as

$$\sigma_I^{\rm OM}=(\pi/k_{\rm d}^2)(2I+1)T_I^{\rm OM}\ . \tag{5}$$

As emphasized in the Introduction, a straightforward use of $\sigma_I^{\rm OM}$, or equivalently of $T_I^{\rm OM}$, as the starting point of the SM calculation, makes the theoretical (d,2n) cross section $\sigma_{\rm theor}$ too large. To remove this trouble, we now introduce the DRAF method.

We can begin to explain this method by first noting that the right-hand side (rhs) of Eq. (4) includes an integral over r that ranges from 0 to infinity. In practice, however, this is a finite-range integral, because the integrand becomes negligibly small beyond a fixed value of r, $R_{\rm max}$, due to the finite-range nature of $W(r)$. Let us now introduce a cutoff radius R_F that is somewhat smaller than $R_{\rm max}$, and define a new transmission coefficient T_I^F as

$$T_I^F=(8/\hbar v_{\rm d})\int_0^{R_F}|\chi_I(r)|^2 W_{\rm d}(r)dr\ . \tag{6}$$

The corresponding cross section σ_I^F may be written, as in (5),

$$\sigma_I^F=(\pi/k_{\rm d}^2)(2I+1)T_I^F\ . \tag{7}$$

The superscript F attached to T_I^F and σ_I^F, and the subscript F attached to R_F, both signify the relation of these quantities to the fusion part of the total reaction cross section.

The use of the DRAF method means that T_I^F shall be used in place of $T_I^{\rm OM}$ in the SM calculations. Since $R_F<R_{\rm max}$, it is guaranteed that $T_I^F<T_I^{\rm OM}$. An appropriate choice of R_F would thus decrease $\sigma_{\rm theor}$ so that it agrees with $\sigma_{\rm expt}$. The details of this numerical problem are discussed in Sec. III, although we might remark here that an R_F chosen to be independent of I and $E_{\rm d}$ reproduces the excitation function $\sigma_{\rm expt}$ very well.

Thus we know that the DRAF method works nicely. (It also worked surprisingly well in heavy-ion fusion analyses.[2]) The method is, nevertheless, based on a rather *ad hoc* phenomenology, and one may well ask that an *a posteriori* justification be provided. One way to do this is to check whether the direct reaction part $\sigma_R^{\rm DR}$ of σ_R, which is given by

$$\sigma_R^{\rm DR}=\sigma_R-\sigma_R^F\ , \tag{8}$$

is accounted for by a summation of the various calculated cross sections for all possible direct-reaction processes. This consistency check is done in Sec. III D.

We wished to avoid the use of a phenomenological

method to separate the direct reactions from the complete fusion reaction. But its use was necessary because there is no known way to treat this separation microscopically. Among other phenomenological methods, we reject the sharp l-cutoff method as unphysical. The smooth l-cutoff method is similar to our method (see Fig. 5), but it contains two parameters. We prefer our one parameter DRAF method.

B. Breakup and breakup-fusion cross sections

We first write down the triple differential cross section for the EB process.[4,5] It is given by

$$\frac{d^3\sigma^{\mathrm{EB}}}{dE_n d\Omega_n d\Omega_p} = (2\pi/\hbar v_d)\rho(E_n)\rho(E_p) \times |\langle \chi_n^{(-)}\chi_p^{(-)} | V_d | \chi_d^{(+)}\phi_d \rangle|^2 . \quad (9)$$

Here, $\rho(E_n)$ and $\rho(E_p)$ are the phase-space volumes for the outgoing neutron and proton, respectively. Clearly, the relation between the neutron energy E_n and the proton energy E_p can be written as

$$E_n + E_p = E_d - B_d , \quad (10)$$

where E_d is the energy of the deuteron and B_d is the deuteron binding energy. Further, $\chi_d^{(+)}$ is the deuteron distorted wave, as in Eq. (1), while $\chi_n^{(-)}$ and $\chi_p^{(-)}$ are, respectively, the neutron and proton distorted waves. The function ϕ_d stands for the spacial part of the deuteron internal-wave function, while the interaction potential V_d is given by

$$V_d = U_n + U_p - U_d . \quad (11)$$

The symbol U_n represents the optical potential of the neutron relative to the target. The quantities U_p and U_d are defined similarly.

The meaning of Eq. (9) is now evident. It is the well-known DWBA (distorted-wave Born approximation) form of the EB cross section. As remarked earlier, Eq. (9) was derived by assuming that the target stays in its ground state after the onset of the breakup. Thus Eq. (9) is in fact the cross section for the elastic breakup. Equation (10) is also the result of the target ground-state assumption, and the corresponding assumption of elastic breakup will be sustained throughout this paper. (That is, we assume that contributions from inelastic breakup[5] are small.)

A comment on the specific choice of the DWBA interaction made in Eq. (11) is worthwhile. To make this choice of the interaction means that we are using its prior form. Since all the interaction potentials U_n, U_p, and U_d that appear in Eq. (11) are long ranged, the exact-finite-range (EFR) method[8,9] must be used in evaluating the six-dimensional integral that is contained in the matrix element appearing in Eq. (9).

If we are interested only in the EB process, we may take advantage of the prior-post equivalence[8] to replace V_d in Eq. (9) by V_{pn}, the interaction between the neutron and the proton. Since V_{pn} is short ranged, we may use the zero-range (ZR) approximation, and thus drastically simplify the calculation.[3] Unfortunately, however, the use of the post-form interaction V_{pn} in Eq. (9) causes a serious problem (discussed in Refs. 5 and 7) in the ensuing formulation of the BF process. Because of this reason we stay with the prior form, in spite of its complexity.

We next write down the double-differential cross section for the BF process, having in mind the case where the neutron flies away and the proton is absorbed:[4,5]

$$\frac{d^2\sigma^{\mathrm{BF}}}{dE_n d\Omega_n} = (2\pi/\hbar v_d)\rho(E_n)(\langle \psi_p^{(+)} | W_p | \psi_p^{(+)} \rangle/\pi) . \quad (12)$$

Here, W_p is the negative of the imaginary part of U_p.

The wave function $\psi_p^{(+)}$ is used to describe the motion of the proton (to be eventually absorbed) relative to the target. Its explicit form is found by first doing a partial wave expansion in spherical harmonics $Y_{lm}(\hat{\mathbf{r}})$ and radial function $u_{lm}(r)$,

$$\psi_p^{(+)}(\mathbf{r}) = \sum_{lm} (1/r) u_{lm}(r) Y_{lm}(\hat{\mathbf{r}}) , \quad (13)$$

and then noting that the radial part of its wave function satisfies the following inhomogeneous differential equation:

$$\left[\frac{d^2}{dr^2} - \frac{l(l+1)}{r^2} + k_p^2 - (2\mu_p/\hbar^2)U_p \right] u_{lm}(r) = \rho_{lm}(r) . \quad (14)$$

The inhomogeneous (source) term $\rho_{lm}(r)$ is given by

$$\rho_{lm}(r) = r\langle Y_{lm}\chi_n^{(-)} | V_p | \chi_d^{(+)}\phi_d \rangle . \quad (15)$$

In Eqs. (13)—(15), $\mathbf{r}$ denotes the coordinate vector between the proton and the target, $\hat{\mathbf{r}}$ being its angular part. In Eq. (14) μ_p is the reduced mass of the proton, while $k_p^2 = 2\mu_p E_p/\hbar^2$. Finally, the matrix element in Eq. (15) implies a five-dimensional integral that is closely related to the six-dimensional integral of Eq. (9).

To obtain the relation between these two integrals, we first expand into partial waves the proton distorted wave $\chi_p^{(-)}$ that appears in Eq. (9), just as $\psi_p^{(+)}$ was expanded in Eq. (13) above:

$$\chi_p^{(-)}(\mathbf{r}) = (4\pi/k_p r) \sum_{lm} i^l \chi_l(r) Y_{lm}(\hat{\mathbf{r}}) Y_{lm}^*(-\hat{\mathbf{k}}_p) . \quad (16)$$

Here, $\hat{\mathbf{k}}_p$ denotes the angular part of the proton momentum $\mathbf{k}_p$, i.e., $\hat{\mathbf{k}}_p$ describes the direction into which the proton proceeds (in the EB case).

If Eq. (16) is used, the matrix element in Eq. (9) can be rewritten as

$$\langle \chi_p^{(-)}\chi_n^{(-)} | V_d | \chi_d^{(+)}\phi_d \rangle = (4\pi/k_p) \sum_{lm} i^l Y_{lm}^*(-\hat{\mathbf{k}}_p) \int \chi_l(r) r \langle Y_{lm}\chi_n^{(-)} | V_d | \chi_d^{(+)}\phi_d \rangle dr . \quad (17)$$

Equation (17) clearly establishes the relation between the two matrix elements, i.e., between the six- and five-dimensional integrals. It also clarifies the meaning of the source term $\rho_{lm}(r)$. The source of this proton motion has indeed been created by the EB process that occurred as the first step of the BF reaction.

Once $\rho_{lm}(r)$ is obtained, it can be used in Eq. (17) to complete the calculation of the breakup cross section of Eq. (9). By using the same $\rho_{lm}(r)$ in Eq. (14), the inhomogeneous equation is solved with the outgoing-wave boundary condition to obtain $u_{lm}(r)$. The latter is used in Eq. (13) to obtain the wave function $\psi_{\rm p}^{(+)}(r)$, which is, in turn, used in Eq. (12) to finally obtain the BF cross section. [See Ref. 10 for an explicit form of $\rho_{lm}(r)$.]

It is convenient to write down explicitly the result of inserting Eq. (13) into Eq. (12). It may be written as

$$\frac{d^2\sigma^{\rm BF}}{dE_{\rm n}d\Omega_{\rm n}}=\sum_l \frac{d^2\sigma_l^{\rm BF}}{dE_{\rm n}d\Omega_{\rm n}} , \tag{18a}$$

with

$$\frac{d^2\sigma_l^{\rm BF}}{dE_{\rm n}d\Omega_{\rm n}}=\sum_m (2/\hbar v_{\rm d})\rho(E_{\rm n})\int |u_{lm}(r)|^2 W_{\rm p}(r)dr . \tag{18b}$$

Note that $\rho_{lm}(r)$ depends on $\hat{\mathbf{k}}_{\rm n}$ via the $\hat{\mathbf{k}}_{\rm n}$ dependence of $\chi_{\rm n}^{(-)}$ [cf. Eq. (15) and Eq. (16)]. The radial wave function $u_{lm}(r)$ thus depends on $\hat{\mathbf{k}}_{\rm n}$, as seen from Eq. (14). This is why the rhs of Eq. (18b) depends on $\hat{\mathbf{k}}_{\rm n}$, i.e., on $\Omega_{\rm n}=(\theta_{\rm n},\phi_{\rm n})$. [Because of the axial symmetry of the whole problem, the rhs of Eq. (18b) is, in fact, independent of $\phi_{\rm n}$.] The function $u_{lm}(r)$ also depends on $E_{\rm p}$, as seen from Eq. (14). Since $E_{\rm n}$ is uniquely related to $E_{\rm p}$ by Eq. (10), $u_{lm}(r)$, and hence the rhs of Eq. (18b) also depends on $E_{\rm n}$.

The derivation of Eq. (18) completes the derivation of the breakup-fusion cross section.

C. Statistical model calculation

We now discuss how to use the results of subsections A and B for the new calculation of the statistical processes.

The application of the result of subsection A should be evident. It is essentially the same as that for the SSM calculation, in which the complete fusion of the deuteron with the target is assumed. The only difference is that we should now use the transmission coefficients T_l^F given in Eq. (6), rather than $T_l^{\rm OM}$ given in Eq. (4). We denote by $\sigma^F(i)$ the formation cross sections of the i ($i=6^+$ and 2^+) states of ^{52}Mn thus obtained.

In order to explain how to use the result of subsection B, we first note that the BF cross section of Eq. (18) depends on $E_{\rm n}$ and $\theta_{\rm n}$. However, we are not interested in the $\theta_{\rm n}$ dependence, and thus we obtain as the angle integrated cross section:

$$\sigma^{\rm BF}(E_{\rm p})=\sum_I \sigma_I^{\rm BF}(E_{\rm p})=\sum_I 2\pi\int\left[\frac{d^2\sigma_I^{\rm BF}}{dE_{\rm n}d\Omega_{\rm n}}\right]\sin\theta_{\rm n}d\theta_{\rm n} . \tag{19}$$

[$\sigma^{\rm BF}(E_{\rm p})$ is an abbreviation for $d\sigma^{\rm BF}(E_{\rm p})/dE_{\rm p}$.]

Note that the left-hand side of (19) is written as a function of $E_{\rm p}$ rather than $E_{\rm n}$ (as we have written it before in subsection B). This is because the compound nucleus (^{53}Mn*) that results from the BF process of subsection B is the same as that obtained when a proton with an energy $E_{\rm p}$ is absorbed by the target ^{52}Cr. In other words, the SM calculation which we are to perform is essentially the same as that done in Ref. 1 for the (p,n) case. For this reason, we also used I, instead of l, in denoting the spin of the compound state (as we did in subsection A).

Contrary to the actual (p,n) analysis, in which the formation cross section of the spin state I is given by the optical model $\sigma_I^{\rm OM}$ of Eq. (5), the formation cross section in our calculation is given by $\sigma_I^{\rm BF}(E_{\rm p})$ of Eq. (19). To use this formation cross section is, of course, the same as using the transmission coefficient given by

$$T_I^{\rm BF}(E_{\rm p})=(k_{\rm p}^2/\pi)(2I+1)^{-1}\sigma_I^{\rm BF}(E_{\rm p}) . \tag{20}$$

Whether one prefers the use of $\sigma_I^{\rm BF}(E_{\rm p})$ or $T_I^{\rm BF}(E_{\rm p})$, the SM calculation that is to be performed should be evident. Let us denote the formation cross section of the i state thus obtained by $\sigma^{\rm BF}(E_{\rm p},i)$.

Obtaining these cross sections is not the end of the present work, however. We are interested in obtaining the BF contribution to the (d,2n) cross section as a function of $E_{\rm d}$. However, for a given $E_{\rm d}$, $E_{\rm p}$ ranges from 0 to $E_{\rm d}-B_{\rm d}$; see Eq. (10). The cross section we want then is given by

$$\sigma^{\rm BF}(i)=\int_0^{E_{\rm d}-B_{\rm d}}\sigma^{\rm BF}(E_{\rm p},i)dE_{\rm p} . \tag{21}$$

III. NUMERICAL CALCULATIONS

Three types of calculations are discussed for the analysis of the ^{52}Cr(d,2n)^{52}Mn^{g,m} data. The first is the standard SM, i.e., the Hauser-Feshbach plus preequilibrium-type calculation. We refer to the result of this calculation as the SSM (standard SM) result. The second calculation is performed using the DRAF method of Sec. II A, and the result of this calculation is referred to as the DRAF result. The third calculation is based on the BF theory. The result of this calculation together with the calculation of the evaporation of a neutron from ^{53}Mn is referred to as the BFE result.

Since details of the SM calculation have been reported in Ref. 1, its explanation here will be brief.

A. Standard statistical model (SSM) calculations

The SM part of the calculation is involved in all the SSM, DRAF, and BFE calculations. We used the current Livermore version of the statistical model code STAPRE,[11] which is designed to calculate energy-averaged cross sections for particle-induced reactions. The reaction is assumed to proceed first by emitting preequilibrium particle in accordance with the exciton model.[12] This emission is followed by the evaporation of equilibrated particles and then by the emission of gamma rays. These latter processes are treated in terms of the Hauser-Feshbach for-

malism with conservation of angular momentum and parity.[13]

The results of the SSM calculations have been reported in Ref. 1 and are summarized as follows: For the (p,n) case, we were able to reproduce the cross section $\sigma=\sigma(g)+\sigma(m)$ and the isomer ratio $R=\sigma(m)/\sigma(g)$ with good accuracy. However, for the (d,2n) reaction, the cross section which we now denote by $\sigma_{\rm SSM}$ is too large by 30—50%, while the isomer ratio which we denote by $R_{\rm SSM}$ is too small by about a factor of 2. These troubles are clearly seen in Figs. 1 and 2, where $\sigma_{\rm SSM}$ and $R_{\rm SSM}$ are compared with respective experimental values.[1]

Note that the SSM results refer to the following choices of preequilibrium model parameters: the parameter $K=200$ MeV^3, a constant that defines the average two-body residual interaction in the preequilibrium model, and two particle—one hole as initial exciton configuration. We point out that both the quantity K and the initial exciton configuration are treated as free parameters. The choice of a two particle—one hole initial configuration is arbitrary, but our conclusion of the companion paper on the isomer ratio is unaffected by the choice of the initial configuration.

We also point out here that an adjustment of the level densities and the compound/precompound fraction can force the $\sigma_{\rm SSM}$ to become closer to $\sigma_{\rm expt}$, but they affect $R_{\rm theor}$ only negligibly. An adjustment of the gamma branching ratios in ^{52}Mn can change $R_{\rm theor}$, but once this change is made, the good agreement with data already achieved for the (p,n) case is completely destroyed.

We thus have to look for a new mechanism which makes $\sigma_{\rm theor}$ and $R_{\rm theor}$ agree with experimental (d,2n) results, without appealing to these adjustments.

This is why we carry out the DRAF and BFE calculations in the next two subsections. In presenting the results of these calculations, we find it convenient to define $\sigma_{\rm DRAF}$ and $R_{\rm DRAF}$ as

$$\sigma_{\rm DRAF}=\sigma^F(g)+\sigma^F(m)\ , \tag{22a}$$

$$R_{\rm DRAF}=\sigma^F(m)/\sigma^F(g)\ . \tag{22b}$$

The formation cross section, $\sigma^F(i)$, was defined at the beginning of Sec. II C. Note also that $\sigma^F(i)$, and hence $\sigma_{\rm DRAF}$ and $R_{\rm DRAF}$, are functions of the cutoff radius R_F. If R_F is taken to be equal to infinity, $\sigma_{\rm DRAF}$ and $R_{\rm DRAF}$ reduce, respectively, to $\sigma_{\rm SSM}$ and $R_{\rm SSM}$.

Corresponding to Eqs. (22a) and (22b), we may also define $\sigma_{\rm BFE}$ and $R_{\rm BFE}$ as

$$\sigma_{\rm BFE}=\sigma^{\rm BF}(g)+\sigma^{\rm BF}(m)\ , \tag{23a}$$

$$R_{\rm BFE}=\sigma^{\rm BF}(m)/\sigma^{\rm BF}(g)\ , \tag{23b}$$

where $\sigma^{\rm BF}(i)$ was defined in Eq. (21). We shall also need definitions for $\sigma_{\rm theor}$ and $R_{\rm theor}$:

$$\sigma_{\rm theor}=\sigma_{\rm DRAF}+\sigma_{\rm BFE}\ , \tag{24a}$$

$$R_{\rm theor}=[\sigma^F(m)+\sigma^{\rm BF}(m)]/[\sigma^F(g)+\sigma^{\rm BF}(g)]\ . \tag{24b}$$

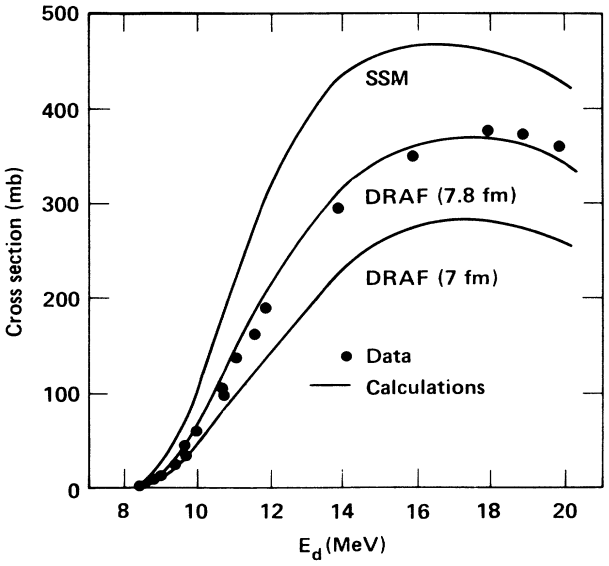

FIG. 1. Comparison of the calculated total cross sections $[\sigma(g)+\sigma(m)]$ with experimental data (Ref. 1) for the reaction ^{52}Cr(d,2n)^{52}Mn^{g,m}. The calculated results of the DRAF and SSM methods are identified. E_d is the bombarding energy.

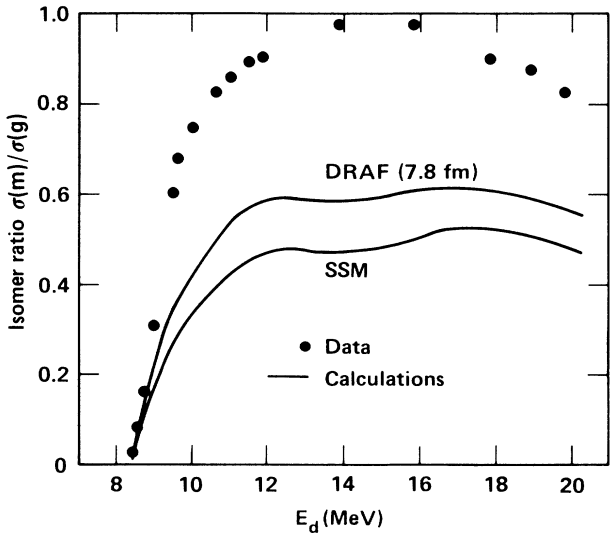

FIG. 2. Comparison of the calculated isomer ratio $[\sigma(m)/\sigma(g)]$ with measured data of Ref. 1 for the reaction ^{52}Cr(d,2n)^{52}Mn^{g,m}.

B. Statistical model calculations with the DRAF method

We now use the DRAF method of Sec. II A to generate the entrance-channel spin distribution for the ensuing SM calculations. As we stressed in Sec II A, every calculation is the same as that done with the SSM method in Sec. III A, except for the use of the transmission coefficient T_l^F of Eq. (6) instead of $T_l^{\rm OM}$ of Eq. (4). In all of our calculations, we used the Moldauer potential[14] for neutrons below 1 MeV and the Rapaport potential[15] above 1 MeV. For protons we use the global potential of Perey[16] and for

alpha particles the McFadden-Satchler potential.[17] The deuteron potential is used without the spin-orbit term (see discussion in Sec. II A); we have used the potentials from Lohr and Haeberli[18] below 13 MeV and Perey and Perey[19] above 13 MeV. The choice of the above optical potentials has been discussed in the companion paper. Here we simply mentioned them for completeness.

The results of the calculations using the DRAF method are shown in Figs. 1 and 2. In Fig. 1 we compare $\sigma_{\rm SSM}$ and $\sigma_{\rm DRAF}$ with experimental data. The disagreement with $\sigma_{\rm SSM}$, i.e., with $\sigma_{\rm DRAF}$ for $R_F=\infty$, is evident. The line denoted by DRAF (7.8 fm) represents the $\sigma_{\rm DRAF}$ cross section of Eq. (22) obtained with $R_F=7.8$ fm and fits the data quite well. Figure 1 also presents the result obtained with $R_F=7$ fm. This result is given to provide an idea about the cross section variation with R_F. Additional information about this variation is found in Fig. 3 and will be discussed shortly.

In Fig. 2 the isomer ratio R is given both for SSM ($R_F=\infty$) and DRAF ($R_F=7.8$ fm). It can be seen that a significant improvement has been achieved by using a finite value of R_F.

The reason that the use of a finite R_F improves the fit to the σ data is simply a consequence of the fact that $T_I^F < T_I^{\rm OM}$, as was stressed in Sec. II A. The reason the fit to R data is also improved is that the spin distribution has shifted to lower values of I, i.e., the ratio $T_I^F/T_I^{\rm OM}$ gets smaller as I grows larger. Since the isomeric state has a lower spin (2^+) than the ground state (6^+), the resulting lower spin distribution helps to increase R.

Although the DRAF result shown in Fig. 1 with $R_F=7.8$ fm fits the σ data nicely, we cannot take it as our final result because there are also BFE contributions to σ. To accomodate the latter we calculated $\sigma_{\rm DRAF}$ once again, this time for $R_F=7.3$ fm. The result of the calculation is given in Fig. 3. We note that it underestimates $\sigma_{\rm expt}$. To this $\sigma_{\rm DRAF}$, we add $\sigma_{\rm BFE}$, to obtain the final calculated cross section. Both $\sigma_{\rm BEF}$ and $\sigma_{\rm DRAF}$ and their sum are shown in Fig. 3. The calculation of $\sigma_{\rm BFE}$ is discussed in the next subsection.

Corresponding results for the isomer ratio are presented in Fig. 4. We postpone discussion of this figure to the next subsection.

C. Breakup-fusion evaporation (BFE) calculations

This is the most time consuming part of the whole calculation because once the bombarding energy $E_{\rm d}$ is chosen, $E_{\rm n}$ must range from 0 to $E_{\rm d}-B_{\rm d}$, as seen in (10). We chose ten equally spaced values of $E_{\rm n}$ in this range, and performed the BF calculations separately for each pair of $E_{\rm d}$ and $E_{\rm n}$. Since we chose eight values for $E_{\rm d}$ (9, 10, 12.5, 15, 17.5, 20, 25, and 30 MeV), we had 80 sets of $E_{\rm d}$ and $E_{\rm n}$ values altogether. For each of these sets, we calculated $\rho_{lm}(r)$ for $l=0$—10 and $m=0$ and 1, and for a particular range of r. Note that the experimental data on the (d,2n) reaction are available only up to $E_{\rm d}\cong 20$ MeV.

The calculation of EB and BF cross sections after obtaining $\rho_{\rm lm}(r)$ has been explained in Sec. II B. Obtaining the BF contribution to the (d,2n) cross section, i.e., calculating $\sigma^{\rm BF}(i)$, was then explained in Sec. II C [see Eq. (21) in particular]. As remarked above, we wish to obtain $\sigma_{\rm BFE}$ and $R_{\rm BFE}$ as they are defined by Eq. (23). Note that in the EB and BF calculations, the spin-orbit term of the optical potentials (Refs. 14—16 and 18—21) are ignored. The spin-orbit terms, however, are included in the evaporation part of the calculation.

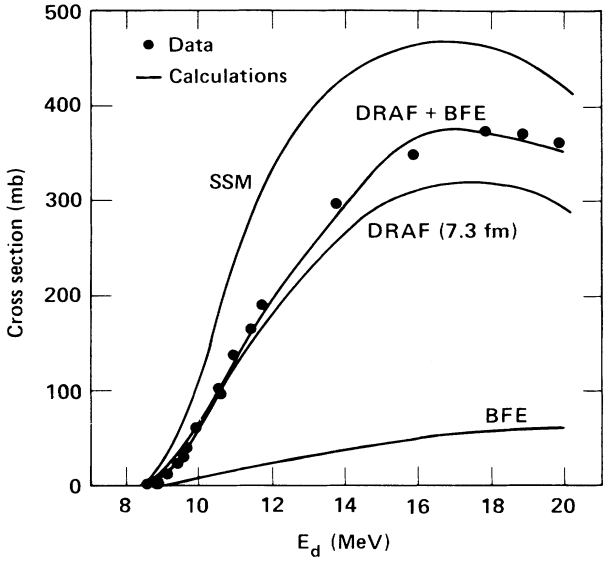

FIG. 3. Total reaction cross section [i.e., $\sigma(g)+\sigma(m)$] for the reaction ^{52}Cr(d,2n)^{52}Mn^{g,m}. The combined results of DRAF and BFE are compared with the experimental data of Ref. 1. The SSM results are also shown for comparison.

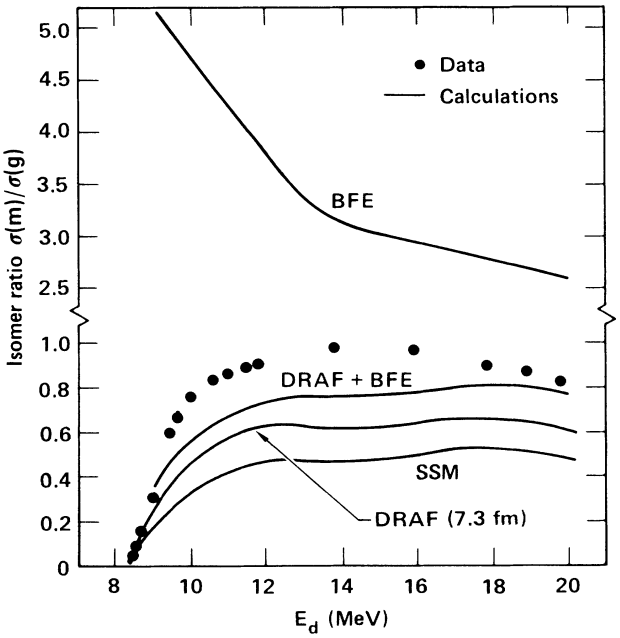

FIG. 4. Isomer ratio $[\sigma(m)/\sigma(g)]$ for the reaction ^{52}Cr(d,2n)^{52}Mn^{g,m}. The combined results of DRAF and BFE are compared with the data of Ref. 1. The SSM results are also shown for comparison.

The $\sigma_{\rm BFE}$ is plotted in Fig. 3 as a function of $E_{\rm d}$, and so is the $\sigma_{\rm DRAF}$ obtained for $R_F=7.3$ fm. The sum of these two gives $\sigma_{\rm theor}$ [Eq. (24a)], which, as seen in the figure, reproduces the experimental cross section $\sigma_{\rm expt}$ very nicely. This fit to the data is a major success of the approach we have employed.

$R_{\rm BFE}$ and $R_{\rm theor}$ are given, along with $R_{\rm DRAF}$, in Fig. 4. One can see that $R_{\rm BFE}$ is larger than unity for all $E_{\rm d}$ and that it is particularly large at lower $E_{\rm d}$. However, the final theoretical $R_{\rm theor}$ is calculated by Eq. (24b). Since $\sigma^{\rm BF}(i) \ll \sigma^F(i)$, as seen from Fig. 3, the large $R_{\rm BFE}$ does not produce very large $R_{\rm theor}$, although it certainly helps to make $R_{\rm theor}$ larger than $R_{\rm DRAF}$. The $R_{\rm theor}$ now agrees rather well with $R_{\rm expt}$, as seen in Fig. 4, although it is still somewhat too small. Nonetheless, the improvement of $R_{\rm theor}$ as compared with $R_{\rm SSM}$ is clearly evident.

In subsection B, we discussed the fact that the calculated value of R increases if the spin distribution is decreased. To give a more quantitative idea of the process, we present in Fig. 5 the spin distributions for the SSM, DRAF, and BFE cases for $E_{\rm d}=15$ MeV. More precisely, for the SSM and DRAF cases we plot the cross sections $\sigma_I^{\rm OM}$ [of Eq. (5)] and σ_I^F [of Eq. (7) for $R_F=7.3$ fm] with which the spin state I of ^{54}Mn is formed. For the BFE case the cross section $\sigma_I^{\rm BF}(E_{\rm p})$ of Eq. (19) is plotted after it has been integrated over $E_{\rm p}$ from 0 to $E_{\rm d}-B_{\rm d}$. This BFE curve thus gives an idea of the cross section with which the spin state I of ^{53}Mn is formed.

The shift to the lower spin distribution in using DRAF rather than SSM is not very large, yet it is sufficient to increase R from $R_{\rm SSM}\cong 0.5$ to $R_{\rm DRAF}\cong 0.6$. On the other hand, the spin distribution of BFE is very strongly shifted to the lower spins, which explains the very large $R_{\rm BFE}$ seen in Fig. 4.

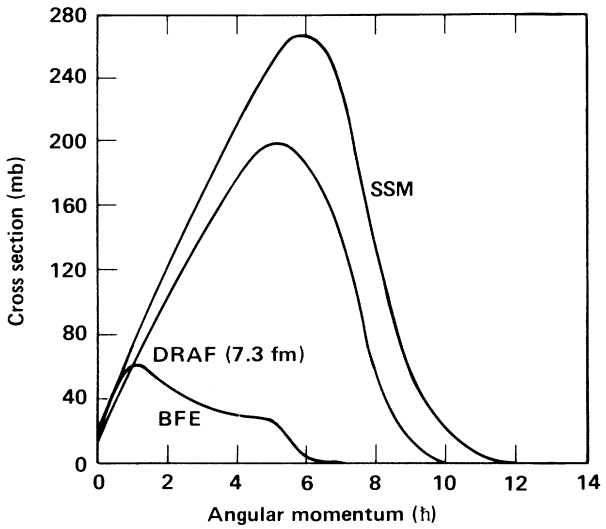

FIG. 5. Spin distributions for the SSM, DRAF, and BFE methods for 15 MeV deuteron incident on ^{52}Cr.

D. Check of consistency

At the start of the present analysis we divided the total reaction cross section σ_R into two parts, σ_R^F and $\sigma_R^{\rm DR}$, and retained only σ_R^F as the part contributing to the complete fusion of the deuteron. We have made this division phenomenologically, and we now want to perform a consistency check to justify the division. We wish to show that the part $\sigma_R^{\rm DR}$ that was left over in the above complete-fusion calculation can, in fact, be understood as the direct reaction part of σ_R.

Our result is summarized in Table I: It lists various cross sections obtained for seven $E_{\rm d}$ values given in column 1. In columns 2 and 3, respectively, we give σ_R and $\sigma_R^{\rm DR}$ (defined as $\sigma_R-\sigma_R^F$, with σ_R^F being calculated for $R_F=7.3$ fm). In column 4, we give the total EB cross section $\sigma_{\rm EB}$, which was obtained by integrating the EB cross section of Eq. (9) over $\Omega_{\rm p}$, $\Omega_{\rm n}$, and $E_{\rm n}$. The total BF cross section for the neutron, $\sigma_{\rm BF}^{(\rm n)}$, in column 5, was obtained by integrating the BF cross section of Eq. (12) over $\Omega_{\rm n}$ and $E_{\rm n}$. By assuming that the corresponding BF contribution to the proton singles cross section is the same as that of the neutron $\sigma_{\rm BF}^{(\rm n)}$, we listed in column 6 the total breakup-related cross section σ_B, which equals $\sigma_{\rm EB}+2\sigma_{\rm BF}^{(\rm n)}$.

Since σ_B is expected to account for the major part of $\sigma_R^{\rm DR}$, the required confirmation of the consistency is accomplished by confirming that $\sigma_B\cong\sigma_R^{\rm DR}$ (cf. columns 3 and 6). We also give in column 7 the ratio $(\sigma_R^{\rm DR}-\sigma_B)/\sigma_R$, which is a measure of the violation of the consistency. The smallness of the entries in column 7 confirms that our analysis was done in a consistent manner. [The sharp change in $(\sigma_R^{\rm DR}-\sigma_B)/\sigma_R$ from 12.5 to 15 MeV, as seen in the table, is a consequence of the two choices of the deuteron potentials made in this calculation. Note that we have used Lohr-Haeberli potential[18] below 13 MeV and the Perey-Perey potential[19] above 13 MeV.]

Our choice of the optical potentials has been carried over from the companion paper. However, in order to test the sensitivity of σ_B to different choices of optical potentials, we performed additional calculations with deuteron potentials of Lohr and Haeberli[18] and Daehnick *et al.*,[20] and the neutron and proton potentials of Becchetti and Greenlees[21] for a fixed deuteron bombarding energy of 15 MeV. The results show a 7% variation with respect to the three deuteron potentials and a 16% variation with respect to the different neutron and proton potentials. We believe that further choice of appropriate optical potentials will lead to similar variations, and thus our conclusions are not likely to be altered.

IV. SUMMARY AND DISCUSSIONS

The data of the ^{52}Cr(d,2n)^{52}Mn^{g,m} reaction[1] was analyzed. Since the standard statistical model (SSM) could not explain the (d,2n) data, we chose an approach quite different from that of SSM.

Our approach was to emphasize the direct-reaction aspects involved in deuteron induced reactions. We began by recognizing that the direct-reaction part $\sigma_R^{\rm DR}$ of the total-reaction cross section σ_R should not be included in

TABLE I. Various cross sections for the deuteron induced reaction on ^{52}Cr: σ_R (total reaction cross section), σ_R^{DR} (direct reaction part of σ_R calculated with $R_F=7.3$ fm), σ_{EB} (elastic breakup cross section), $\sigma_{\mathrm{BF}}^{(\mathrm{n})}$ (breakup fusion contribution to neutron singles cross section), and σ_B (total breakup cross section, $\sigma_B=\sigma_{\mathrm{EB}}+2\sigma_{\mathrm{BF}}^{(\mathrm{n})}$.

E_{d}(lab) (MeV)	σ_R (mb)	σ_R^{DR} (mb)	σ_{EB} (mb)	$\sigma_{\mathrm{BF}}^{(\mathrm{n})}$ (mb)	σ_B (mb)	$\frac{\sigma_R^{\mathrm{DR}}-\sigma_B}{\sigma_R}$
10	1388	596	34	163	360	0.17
12.5	1525	614	52	176	404	0.14
15	1547	464	61	178	417	0.03
17.5	1599	466	65	175	415	0.03
20	1635	467	67	170	407	0.04
25	1680	465	70	159	388	0.05
30	1707	463	66	149	364	0.06

the formation cross section of ^{54}Mn as is usually done in SSM. Only the internal part σ_R^F of σ_R should be considered as the cross section that leads via ^{54}Mn to the eventual formation of ^{52}Mn. At the same time, we recognize that the breakup-fusion process whose cross section is a part of σ_R^{DR} contributes to the formation of ^{52}Mn. This process first creates ^{53}Mn*, which can then partially decay into ^{52}Mn. We found that, when summed, the contributions from these two processes give a good fit to the data of Ref. 1.

Since the separation of σ_R^F from σ_R was done phenomenologically, we wished to make an *a posteriori* justification. This we did by confirming that the σ_R^{DR} part of σ_R was well accounted for by the sum of the various breakup-related direct-reaction cross sections.

In defining the SSM model, we used 2p-1h as the initial exciton configuration in the preequilibrium model. This is carried over from the companion, experimental paper, where initial exciton configuration is treated strictly as a parameter. However, we point out that our conclusions of this paper would not be affected by the 3p-1h configuration, but would be affected by the 2p-0h configuration.

The problems of "complete fusion" and "incomplete fusion" (the latter being synonymous with breakup fusion) have been fashionable subjects of study in recent years in the field of heavy-ion reactions.[2,22] Considering this heightened interest in heavy-ion reactions, it is somewhat surprising to find that not much corresponding work has been done in the field of light-ion induced reactions. The data of Ref. 1 gave us an excellent opportunity to fill in this gap.

We should emphasize that the data of Ref. 1 contains (p,n) data as well, with the same target and the same final nucleus. The requirement that the two sets of data should be analyzed consistently sets an additional constraint and made the present analysis more meaningful and convincing.

ACKNOWLEDGMENTS

We acknowledge helpful discussions with H. I. West, Jr., R. G. Lanier, and M. Blann. This work was performed under the auspices of the U. S. Department of Energy at the Lawrence Livermore Laboratory under Contract No. W-7405-ENG-48 and at the University of Texas at Austin under Grant No. DE-FG05-84ER40145.

*Permanent address: Department of Physics, University of Texas, Austin, TX 78712.

[1]H. I. West, Jr., R. G. Lanier, and M. G. Mustafa, preceding paper, Phys. Rev. C **35**, 2067 (1987).

[2]T. Udagawa, B. T. Kim, and T. Tamura, Phys. Rev. C **32**, 124 (1985); B. T. Kim, T. Udagawa, and T. Tamura, *ibid.* **33**, 370 (1986).

[3]G. Bauer, M. Pauli, F. Rosel, and D. Trautmann, Nucl. Phys. **A315**, 241 (1979); A. Kasano and M. Ichimura, Phys. Lett. **115B**, 81 (1982).

[4]T. Udagawa and T. Tamura, Phys. Rev. C **24**, 1348 (1981).

[5]T. Udagawa and T. Tamura, Phys. Rev. C **33**, 494 (1986).

[6]T. Udagawa, D. Price and T. Tamura, Phys. Lett. **118B**, 45 (1982); T. Udagawa, X.-H. Li, and T. Tamura, *ibid.* **135B**, 333 (1984); **143B**, 15 (1984); X.-H. Li, T. Udagawa, and T. Tamura, Phys. Rev. C **30**, 1349 (1984).

[7]X.-H. Li, T. Udagawa, and T. Tamura, Phys. Rev. C **30**, 1895 (1984).

[8]G. R. Satchler, *Direct Reaction Theory* (Oxford University Press, Oxford, 1983).

[9]T. Tamura, Phys. Rep. **14c**, 59 (1974); T. Tamura, Y. Amakawa, and T. Udagawa, Prog. Theor. Phys. **60**, 1238 (1978).

[10]R. C. Mastroleo, T. Udagawa, and T. Tamura, Phys. Rev. C (to be published).

[11]D. G. Gardner, Livermore version of a statistical model code originally written by B. Ströhmaier and M. Uhl, Institut für Radiumforschung und Kernphysik (Vienna), Report No. IRK 76/01 with Addenda, 1976.

[12]M. Blann, Annu. Rev. Nucl. Sci. **25**, 123 (1975).

[13]E. Vogt, Adv. Nucl. Phys. **1**, 261 (1968).

[14]P. A. Moldauer, Nucl. Phys. **47**, 65 (1963).

[15]J. Rapaport, Phys. Rep. **87**, 25 (1982).

[16]F. G. Perey, Phys. Rev. **131**, 745 (1963).

[17]L. McFadden and G. R. Satchler, Nucl. Phys. **84**, 177 (1966).
[18]J. M. Lohr and W. Haeberli, Nucl. Phys. **A232**, 381 (1974).
[19]C. M. Perey and F. G. Perey, Phys. Rev. **132**, 755 (1963).
[20]W. W. Daehnick, J. D. Childs, and Z. Vrcelj, Phys. Rev. C **21**, 2253 (1980) (potential 79 DCV,L).
[21]F. D. Becchetti, Jr. and G. W. Greenlees, Phys. Rev. **182**, 1190 (1969).
[22]C. Gerschel, Nucl. Phys. **A387**, 297c (1982); R. H. Siemssen, *ibid.* **A400**, 245c (1983).